Auxetic cementitious composites (ACCs) with excellent compressive ductility Experiments and modeling

Xu, Yading; Šavija, Branko

DOI
10.1016/j.matdes.2023.112572

Publication date
2023

Document Version
Final published version

Published in
Materials and Design

Citation (APA)
Xu, Y., & Šavija, B. (2023). Auxetic cementitious composites (ACCs) with excellent compressive ductility: Experiments and modeling. *Materials and Design*, *237*, Article 112572. https://doi.org/10.1016/j.matdes.2023.112572

Materials & Design 237 (2024) 112572

Contents lists available at ScienceDirect

Materials & Design

journal homepage: www.elsevier.com/locate/matdes

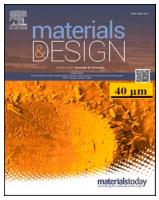

Auxetic cementitious composites (ACCs) with excellent compressive ductility: Experiments and modeling

Yading Xu *, Branko Šavija

Microlab, Civil Engineering and Geosciences, Delft University of Technology, the Netherlands

ARTICLE INFO

Keywords:
Auxetic structures
3D printing
Cementitious composites
Mechanical properties

ABSTRACT

Auxetic cementitious composites (ACCs) with improved mechanical properties are created, by casting 3D printed polymeric auxetic reinforcement structures inside cementitious mortar. Four types of ACCs incorporating reinforcement with different auxetic mechanisms were prepared: "re-entrant" (RE), "rotating-square" (RS), "chiral" (CR) and "missing-rib" (MR). Experiments and finite element models were used to study the compressive behavior of the ACCs. The results indicate that all ACCs have high compressive ductility. Specifically, the RE shows the highest ductility, manifested by 853% and 708% higher energy absorption than the reference mortar and the auxetic structure itself, respectively. In addition, the RE and RS are found to exhibit stronger crack-arresting effect under compression. Therefore, they achieved comparable compressive strength to the reference mortar, which is considerably higher than CR and MR. Furthermore, decreasing the volumetric ratio of the auxetic structure by half, the ductility of the RS reduces by 32.2%, while decreasing the water-to-binder ratio of the cementitious matrix from 0.4 to 0.3 only increases the compressive strength by 18.5%. Moreover, the two-dimensional finite element analyses used herein show a good match with experiments but become less accurate at high strain levels, due to their inability to capture the out-of-plane failure of the ACCs.

1. Introduction

Cementitious materials can achieve good compressive strength at very low cost. The excellent mechanical properties and the ease of manufacturing ensure the wide application of cementitious materials in engineering, for instance, in civil infrastructures. Nevertheless, brittleness is a major drawback of conventional cementitious materials [1,2]. When subjected to external loads, soon after initiation, cracks rapidly propagate through the cementitious material which may eventually result in material failure. Therefore, restricting crack propagation is critical to overcome the brittleness of cementitious materials. For this purpose, numerous studies have been performed aiming to improve the ductility of cementitious materials. For example, steel rebars [3,4] or various types of fibers [5,6] are often used as reinforcement to overcome the brittleness of cementitious materials.

Apart from these traditional methods, in the context of digital manufacturing, cementitious composites incorporating 3D printed structures are also found able to have improved ductility. For example, in our previous work [7], we used 3D printed triangular meshes as reinforcement for cementitious composites that even achieved tensile strain-hardening behavior. In addition, many other 3D printed polymeric structures, for instance octet structures [8,9], minimal-surface structures [10–12] and functionally-graded lattices [13] have also been found able to enhance the cracking resistance of cementitious materials.

In addition to these structures, incorporating auxetic structures in conventional cementitious material may also be a promising approach to create composites with enhanced ductility. Unlike conventional structures, auxetic structures have a fascinating mechanical property: a negative Poisson's ratio [14]: they contract laterally when vertically compressed, or expand laterally when vertically pulled. This unique behavior could potentially allow auxetic structures to limit cracking propagation in cementitious materials under compression, therefore improve the ductility. Moreover, a wide range of auxetic structures have been developed in the past: for instance, "re-entrant" structures [15–18], "chiral" structures [19–21] and "rotating-square" structures [22–24]. A typical feature of the auxetic structures is the highly porous cellular shape. As a result, the compressive strength of auxetic structures is usually much lower than the bulk materials. This significantly limits the total energy absorption of the auxetic structures and their application in

* Corresponding author.
E-mail address: y.xu-5@tudelft.nl (Y. Xu).

https://doi.org/10.1016/j.matdes.2023.112572
Received 30 April 2023; Received in revised form 25 November 2023; Accepted 10 December 2023
Available online 18 December 2023

any load-bearing occasions, even though they are highly deformable. In this sense, taking advantage of the excellent compressive resistance of cementitious material to create composites may also help to overcome the insufficient compressive strength of sole auxetic structures.

Few studies [25–27] have already investigated the potential of using auxetic structures to enhance the mechanical properties of cementitious materials. However, the potential of using auxetic structures to create cementitious composites with enhanced ductility has not been demonstrated yet. Different from polymers and metals, cementitious materials normally exhibit quasi-brittleness under compression. This is determined by the cracking behavior of cementitious materials. On the one hand, though these studies have indicated the potential of auxetic structures to improve ductility of plain cementitious materials, the mechanism of auxetic structure in enhancing the ductility of cementitious materials is still not clarified. On the other hand, compared to the numerous auxetic structures found in literatures [21,22,28,29], the study on the impact of different auxetic mechanisms to enhance the ductility of cementitious materials is still scarce.

The purpose of this work is to create novel auxetic cementitious composites (ACCs) which can reciprocally benefit from the high deformability of auxetic structures and the high compressive strength of cementitious materials. Furthermore, this work aims to understand the performance of ACCs created with four most commonly seen auxetic structures in the literature and clarify the mechanism of achieving excellent mechanical performance. To this end, four types of typical auxetic structures, namely "re-entrant [28]" (RE), "rotating square [22]" (RS), "chiral [29]" (CR) and "missing rib [28]" (MR) structures, were designed. After 3D printed using acrylonitrile butadiene styrene (ABS), these auxetic structures were casted with cementitious mortar to create the ACCs. Subsequently, experimental and numerical studies are performed to obtain in-depth knowledge on the mechanical performance and damage mechanisms of the ACCs.

2. Materials and methods

2.1. Specimen preparation

Cementitious composites with 3D printed polymeric auxetic structures, named herein the auxetic cementitious composites (ACCs) have been fabricated. The cementitious matrix was a fine-grained cementitious mortar containing CEM I 42.5 N and fly ash as binder materials, with water-to-binder ratio (w/b) of 0.3, 0.4 and 0.5. High fluidity was achieved making it easier to fill the hollow cells of the printed auxetic structures. The mixture is given in Table 1.

Although various types of auxetic structures can be found in the literature, most of them either follow single similar original auxetic mechanism or are constructed by combining multiple simple mechanisms. Therefore, in this work, four typical simple auxetic structures: RE, RS, CR and MR, which have different auxetic mechanisms were used. To identify an optimal structure to enhance mechanical properties for ACCs, they were designed to have the same total volume by varying the width of the struts on these structures. The design geometry of the unit cells for the auxetic structures is shown in Fig. 1. The entire auxetic structure were created by duplicating these unit cells and incorporating them in a cementitious mortar to create the ACCs, as shown in Fig. 2. All ACCs specimens have the same dimension of 10 × 40 × 40 mm. The volumetric ratio of each auxetic structure is defined as the percentage volume of the auxetic structure in the total volume of the composite specimen. The volumetric ratio of the RE, RS, CR and MR is 28 %. To study the influence of the volumetric ratio, another series of ACCs (RS14, shown in Fig. 2) with the RS structure was also prepared, in which the auxetic structure has only 5 mm in thickness (i.e., as opposed to 10 mm used in the other series). All designed ACCs are listed in Table 2.

Table 1
Mixture design of the matrix material (g/l).

w/b	CEM I 42.5 N	Fly ash	Sand (0.125 ~ 0.250 mm)	Water	Superplasticizer (Glenium 51)
0.3	526	622	526	344	4
0.4	473	559	473	413	2
0.5	429	507	429	468	0

Polymeric auxetic structures were manufactured using a commercially available fused deposition modeling (FDM) 3D printer Ultimaker 2 +. In FDM, the model is fabricated layer wisely from bottom up. Acrylonitrile Butadiene Styrene (ABS) was used as the printing material. ABS has good mechanical properties and chemical resistance in high alkaline environment, and comparing to conventional steel reinforcement it doesn't corrode when used in cementitious materials. The ABS has been used as reinforcing or toughening phase for cementitious materials [7,8]. As the printing parameters may affect the mechanical properties of the structures [30–32], they were kept constant throughout the entire present work (listed in Table 3). After printing, the auxetic structures were glued by tape in Styrofoam molds (see Fig. 3), preparing for casting.

2.2. Mixing, casting, and curing

Weighted dry materials were first mixed for 4 min, then water and superplasticizer were added, followed by another 4 min of mixing. Subsequently, the fresh mixture was casted in the Styrofoam molds. One day after casting, all specimens were demolded and stored in a curing room (20 ± 2 °C, 96 ± 2 % RH) until the age of 28 days. Before testing, the specimens were cut into desired shape for uniaxial compressive tests.

2.3. Experiments

Uniaxial compression tests were performed on the 3D printed polymeric auxetic structures, as well as the ACCs. As can be seen in Fig. 4a, the surface of the ACCs was painted in white and sprayed with black dots for DIC (digital image correlation) during uniaxial compression test. All uniaxial compression tests were performed under displacement control at a constant loading rate of 0.01 mm/s. The experimental set-up is shown in Fig. 4a. Two steel plates were used to apply force on the specimen. A layer of plastic film was placed between the loading plate and the top/bottom of the specimens to reduce the friction. During the tests, a digital camera was placed in front of the compressed specimen to take photos for DIC analysis.

Uniaxial tensile tests were performed on the cementitious mortar bar (Fig. 4b and c) to obtain tensile properties of the cementitious mortar for the numerical model calibration. The specimen was glued at top and bottom and tested under displacement control at a loading rate of 0.01 mm/s. ABS dog-bone shape bars (see Fig. 5a) were also 3D printed then tested under uniaxial tension to obtain properties for numerical model calibration of the ABS material. The ABS bar was clamped on a small compression-tension stage and tested at a loading rate of 0.01 mm/s. The experimental set-up is shown in Fig. 5b.

3. Numerical modeling

A commercial FEM (finite element modeling) package ABAQUS/Explicit was used to simulate the compressive behavior of the auxetic structures and the ACCs. A plastic material model was used to model the printed ABS structures, and the CDPM [33] (concrete damaged plasticity model) was adopted to simulate the compressive damage of the cementitious composites. As planar specimens were used in the experiment, numerical simulations were also performed using two-dimensional elements to save computational time. Therefore, the out-of-plane properties of the printed ABS structures were not considered in the numerical model, which may introduce potential deviations from

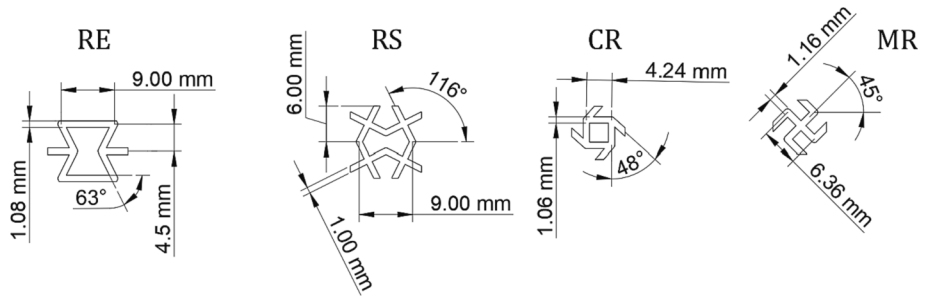

Fig. 1. Design parameters for the four adopted auxetic structures (unit cells).

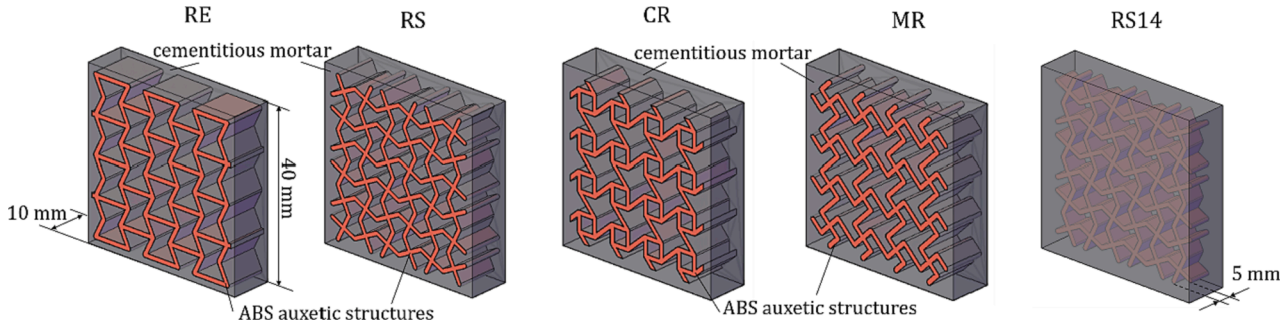

Fig. 2. Schematics of the four types of ACCs to be developed.

Table 2
The volumetric ratio and water-to-binder ratio of the designed ACCs.

Name	Volumetric ratio	Water-to-binder ratio
RE	28 %	0.4
RS	28 %	0.4
CR	28 %	0.4
MR	28 %	0.4
RS14	14 %	0.4
RS14WB3	14 %	0.3
RS14WB5	14 %	0.5

Table 3
Printing parameters.

Parameters	Configuration
Nozzle diameter (mm)	0.6
Temperature (°C)	250
Layer height (mm)	0.15
Line width (mm)	0.53
Infill density (%)	100
Printing speed (mm/s)	40

experimental results. This will be discussed in detail in section 4.

3.1. Concrete damaged plasticity model

The CDPM is a damage based model, which uses E-modulus degradation and plastic strains to simulate the damage process of brittle cementitious materials [34]. It has been proven by various studies [8,33] that the CDPM can properly simulate the damage behavior of cementitious materials under different loading conditions. In this work, the CDPM is used to model the compressive damage of the experimentally tested ACCs. A detailed description of the adopted CDPM can be found in our previous study [33]. Herein, only the material constitutive parameters related to the calibration experiments are introduced. The compressive and tensile constitutive equation can be described as follows:

$$\sigma = (1 - d)E_0(\varepsilon - \varepsilon^{pl}) \quad (1)$$

where σ is Cauchy stress; ε and ε^{pl} are total strain and equivalent plastic strain, respectively; E_0 is initial elastic modulus. In case of E-modulus degradation, d is a damage variable and can be defined from 0 to 1. As shown in Fig. 6, the compressive plastic strain ε_c^{pl} and tensile plastic strain ε_t^{pl} are determined by the stress–strain curve of cementitious

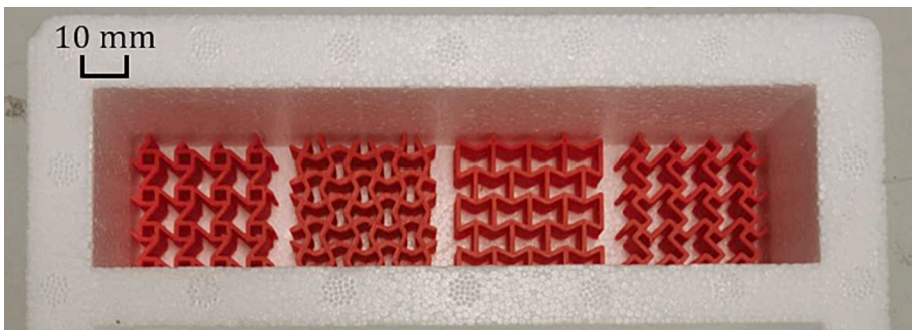

Fig. 3. Auxetic structures placed in Styrofoam mold.

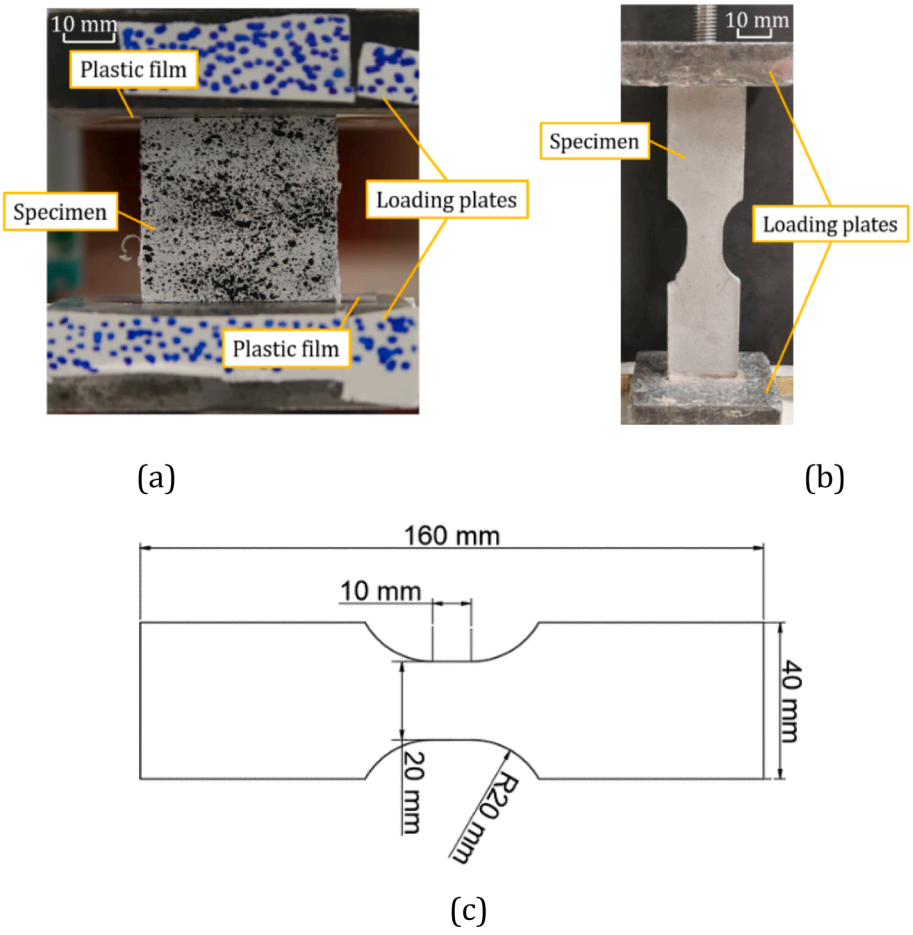

Fig. 4. Experiment set-up for a) uniaxial compression test, b) uniaxial tension test and c) schematics of the cementitious bar.

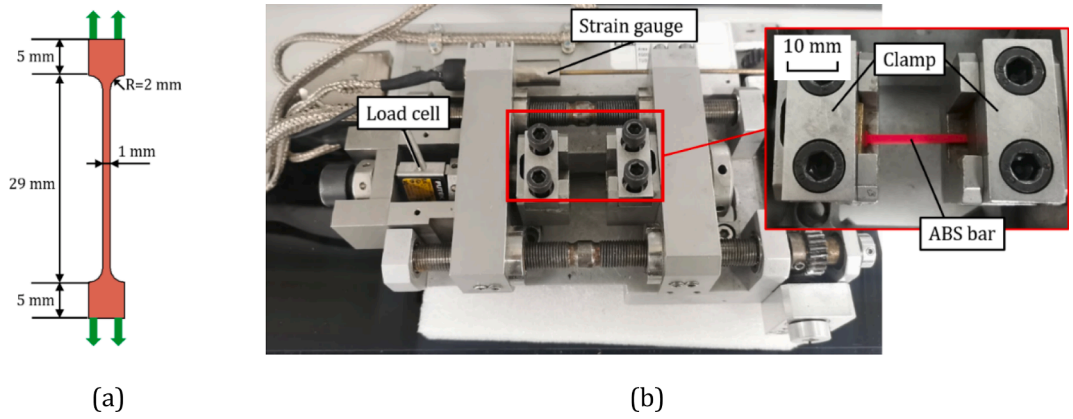

Fig. 5. A) schematics of the ABS dog-bone shape bar, and b) experiment set-up for the ABS bars.

mortar, under uniaxial compression and tension. In compression, the failure stress (σ_{c0}) indicates the onset of mortar micro-cracking after the elastic stage; in tension, the failure stress (σ_{tu}) corresponds to the ultimate tensile strength. The compressive inelastic strain (ε^{in}) and the tensile crack strain (ε^{ck}) is defined as the total strain minus the elastic strain (ε_{c0}^{el} and ε_{t0}^{el}) corresponding to the undamaged mortar [35,36].

3.2. Model calibration

Numerical uniaxial compressive and tensile tests were first performed to calibrate the input parameters for the CDPM. Two-dimensional elements (CPS3 with an average size of 0.5 mm) were used in all FEM models in this work. In the compression model, a minor friction coefficient 0.1 was assigned between the specimens and the loading plates to simulate the low friction condition ensured by the plastic films in the experiment. In addition, this friction coefficient also helps to avoid unrealistic infinite sliding of the specimen in case of pure frictionless condition. A similar approach was also used in several other studies [10,33]. In the uniaxial tension model, the specimen is tied with the loading plates to model the glued boundary used in the experiment. The numerical compression and tension test set-up is shown in Fig. 7.

The material input parameters regulating the compressive and

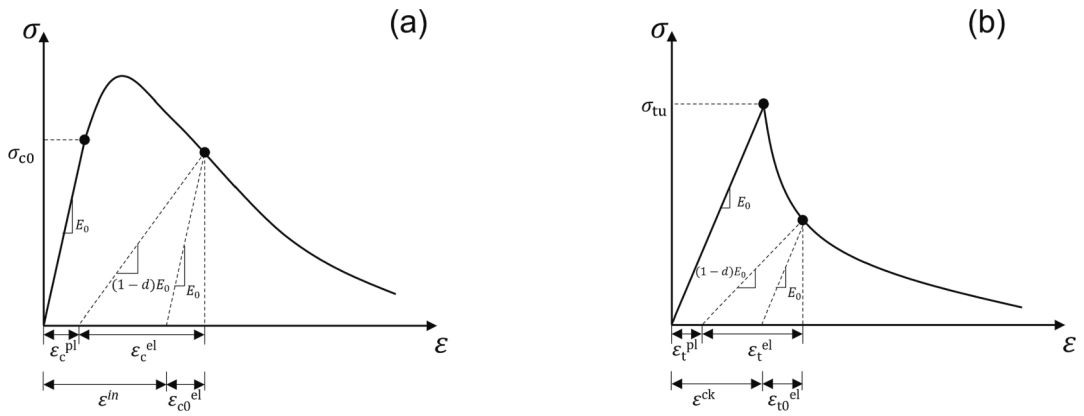

Fig. 6. The constitutive a) compression and b) tension behavior of cementitious mortar in CDPM.

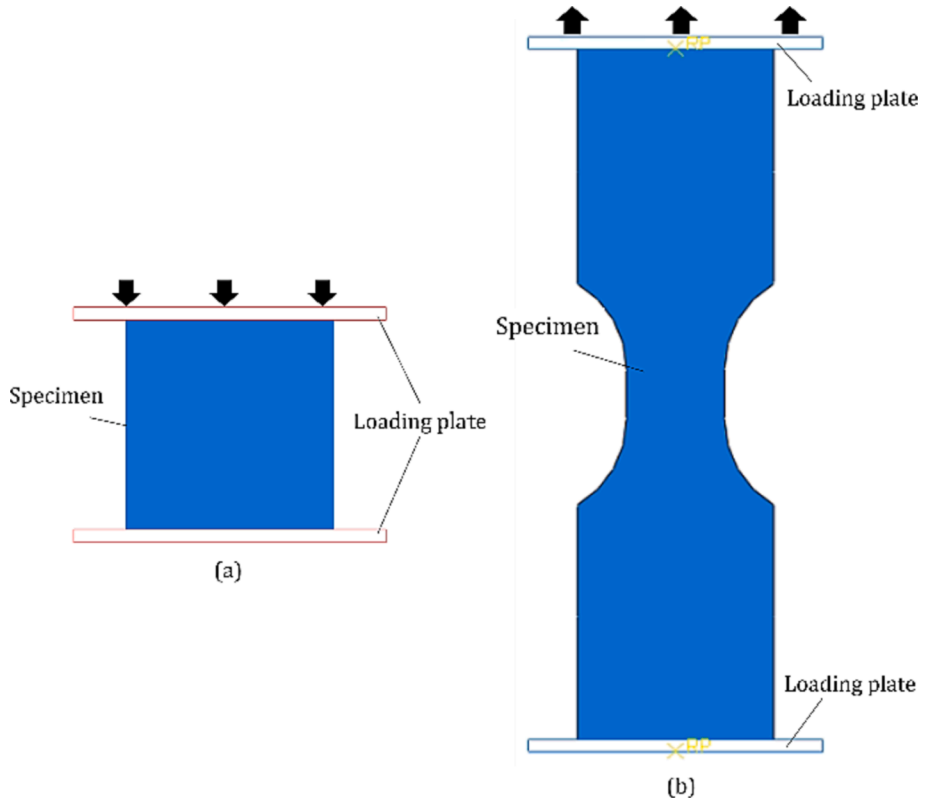

Fig. 7. Numerical a) compression and b) tension test set-up for CDPM calibration.

tensile behavior of the cementitious mortar is listed in Table 4 and Table 5. After the strength, several input points were assumed to ensure computing stability. The other parameters related to the cementitious

Table 4
Compressive behavior input parameters.

Yield Stress (MPa)	Inelastic Strain	Damage Parameter
12	0	0
24	0.0070	0
20	0.0526	0.20
12	0.0576	0.52
10	0.0586	0.60
8	0.0616	0.68
6	0.0636	0.76
3	0.0866	0.88
3	0.2066	0.88

Table 5
Tensile behavior input parameters.

Yield Stress (MPa)	Cracking Strain	Damage Parameter
3.5	0	0
1	0.0014	0.71
0.5	0.0019	0.86
0.3	0.0025	0.91

Table 6
Plasticity input parameters.

Dilation angle	Eccentricity	f_{b0}/f_{c0}	K	Viscosity parameter
35	0.1	1.16	0.667	0.001

mortar plasticity (see Table 6) were adopted from [8], in which a similar plain cementitious mortar was modelled.

The comparison of simulated and experimentally obtained stress–strain curve of the cementitious mortar is shown in Fig. 8. Good agreement is found between the simulation and experiment, which indicates that the numerical model for the cementitious mortar is well calibrated.

For the ABS plastic material model, numerical uniaxial tensile test was also performed to calibrate the material input parameters. A two-dimensional specimen with identical geometry to the experimentally tested ABS dog-bone shape specimens was constructed. The input parameters for the ABS plastic material model are listed in Table 7. The density, elastic modulus and Poisson's ratio of the ABS plastic was 1.07 g/cm^3, 1590 MPa and 0.2, respectively [8]. As seen in Fig. 9, the simulated tensile stress–strain curves also correspond reasonably well to the experiment results, showing that the ABS plastic model is well calibrated.

3.3. Simulation of the compressive experiments

The calibrated models were used to simulate two series of uniaxial compression tests were numerically modelled: the ABS auxetic structures and the ACCs. All four designed auxetic structures and the corresponding ACCs were modelled. Same as the calibration simulation, a minor friction coefficient 0.1 was assigned to prevent unrealistic sliding of the specimens for all simulations. For simulating the ABS auxetic structures, a friction coefficient of 0.75 was arbitrarily assumed. Note that this parameter doesn't influence the simulation results of the ACCs. For the ACCs compression model, a friction coefficient of 1.0 was arbitrarily assumed between the ABS reinforcement and cementitious mortar. Similar arbitrary assumptions can be also seen in previous studies [27,37]. Of course, these interface friction parameters may influence the simulated compressive behavior; however, realistic modelling of the reinforcement/matrix interface is beyond the scope of this study.

4. Results and discussions

4.1. Properties of the ABS auxetic structures

Prior to study the mechanical properties of the ACCs, the compressive deformation and damage behavior of the 3D printed auxetic structures need to be elaborated first. As can be seen in Fig. 10, in general both the simulated stress–strain curves and the deformation process of the auxetic structures are highly in line with the experimental results.

Normally, the compressive damage process of auxetic structures can be classified to characteristic stages as found in plenty studies [15,16,19,33,38], depending on the structure shape, constituent material properties, and the normal strain range. Similar behavior can be also found in this work. Fig. 11 shows the defined stages and terms based on the stress–strain curve obtained by the auxetic structures. In the "stage I", stiffness is defined by the slope of the stress/strain curve. At the end of "stage I", a peak stress is reached. This peak stress is defined as the yield strength [39] of the auxetic structures. It can be found from Fig. 10 that all four auxetic structures follow this two-stages compressive behavior.

The "stage I" corresponds to a yielding process of the auxetic structures. When external load applied, the auxetic structures first deform elastically, witnessed by stress increase with strain at a constant slope on the stress–strain curves. As seen from the deformation pattern (see Fig. 12), within the elastic regime no visible damage can be found in the experiment and simulation yet. The slope of the elastic branch is defined as the stiffness of the auxetic structures. It can be clearly seen from Fig. 13a, according to the experimental results the stiffness of ABS-RE is

Table 7
Input parameters for the ABS plastic.

Yield Stress (MPa)	Plastic Strain
38	0
40	0.6
32	0.7
15	1.0
1	1.2

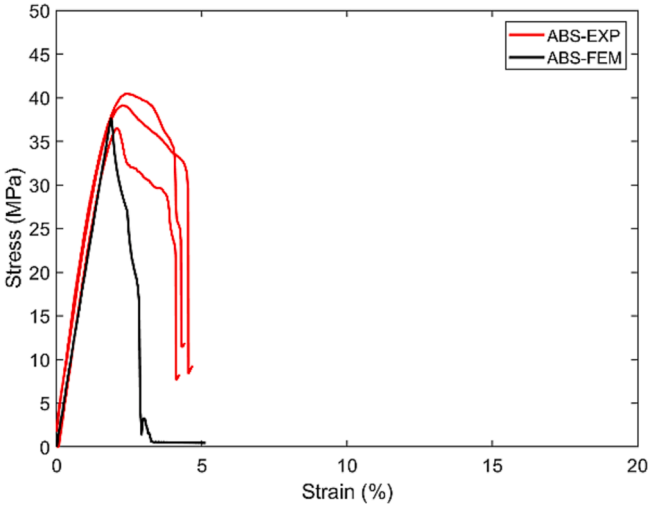

Fig. 9. Calibration results of the ABS bar.

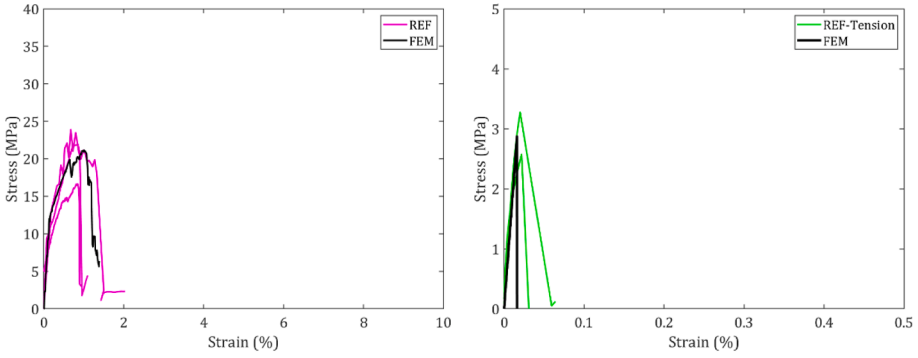

Fig. 8. Calibration results for a) uniaxial compression and b) uniaxial tension, note that the maximum axis value differs in the two figures.

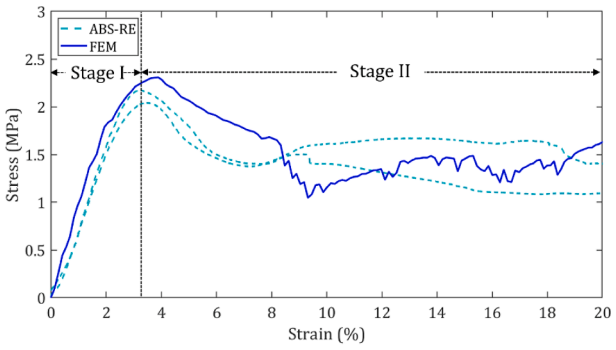

(a)

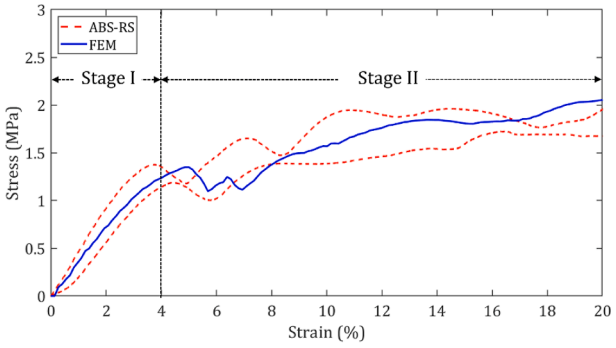

(b)

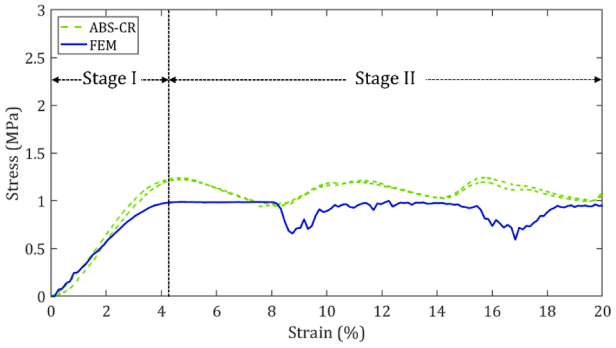

(c)

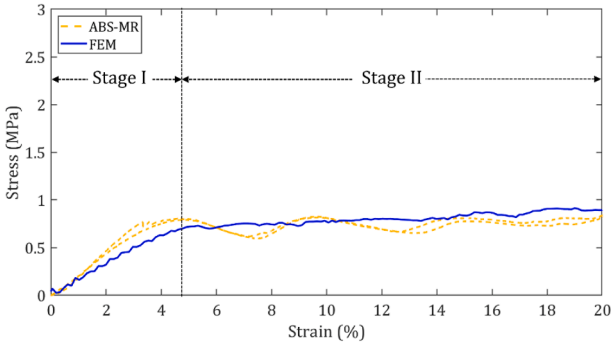

(d)

Fig. 10. Stress–strain curves and the corresponding deformation process of the printed ABS auxetic structures a) ABS-RE, b) ABS-RS, c) ABS-CR and d) ABS-MR.

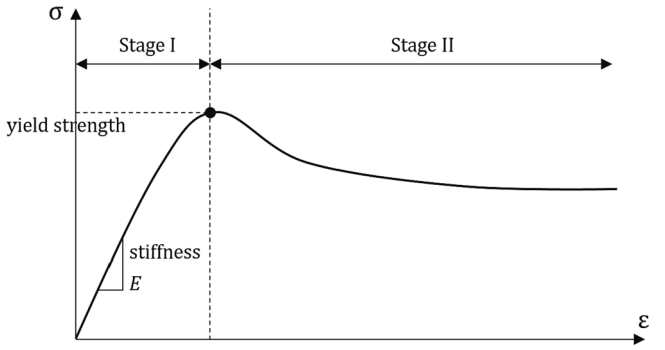

Fig. 11. Typical stress–strain curve of the tested ABS auxetic structure under compression.

82.49 MPa, which is significantly higher stiffness than all other auxetic structures within this stage. The stiffness of ABS-RS, ABS-CR and ABS-MR is 42.30 MPa, 32.19 MPa and 22.26 MPa. They are 48.72 %, 60.98 % and 73.01 % lower than ABS-RE, respectively. The simulation results also indicate a similar trend. At the end of "stage I", a peak stress of is reached. This peak stress is defined as the yield strength [39] of the auxetic structure. As seen in Fig. 13b, the ABS-RE also has the highest yield strength of 2.11 MPa among all four auxetic structures. The ABS-RS and ABS-CR exhibit similar yield strength and they are 39.34 % and 41.71 % lower than ABS-RE, respectively. The yield strength of ABS-MR is only 0.80 MPa. It is significantly lower yield strength than other three auxetic structures. It's worth to notice that, due to the varied cellular structure, there is a very little difference in the strain range of the two stages for the four structures as seen from the stress/strain curves in Fig. 10. For all tested structures, the maximum strain of "stage I" is reached by ABS-MR, at approximately 5 % of strain.

The "stage II" normally indicates that a plateau is present on the stress–strain curve of the auxetic structures [17] as seen in Fig. 10. Within this stage, the cellular units of the printed ABS auxetic structure are gradually compacted. An obvious phenomenon appeared both in the experiment and numerical simulations is the auxetic behavior. This can be seen from Fig. 12: as compressive strain increases, typical lateral contraction is seen from the deformation process of the auxetic structures, meaning that the negative Poisson's ratio is achieved. Therefore, as seen in Fig. 14, experimental tests and numerical simulations indicate similar trends: all auxetic structures exhibited negative Poisson's ratio in this stage, while only the Poisson's ratio of ABS-MR became positive after 15 % of strain. The Poisson's ratio is a critical indicator of the mechanical properties of auxetic structures. It is important to mention that the Poisson's ratios of ABS-RE and ABS-RS are lower than ABS-CR and ABS-MR. This implies that the ABS-RE and ABS-RS may contribute to stronger confinement effect when used in ACCs and ensures the composites better mechanical performance. This effect will be discussed in detail in later sections.

Another significant aspect in "stage II" is the energy absorption ability of the auxetic structures. Corresponding to the long plateau stress–strain curves, the specific energy absorption of all tested auxetic structure increased considerably in "stage II", as seen in Fig. 15. Furthermore, the unit cell shape is found to have huge impact on the energy absorption ability. In sharp contrast to the flat plateau curve of other three structures, the ABS-RS shows even strain-hardening behavior in this stage (see Fig. 10b). This behavior allows the ABS-RS to have significantly improved energy absorption ability. This can be seen in Fig. 15 that, at 20 % strain, the ABS-RS achieved the highest accumulated specific energy absorption (0.0104 J/mm^2) compared to the other three structures, which is approximately 113 % higher than the lowest ABS-MR. The high energy absorption of the ABS-RS may provide greatly enhanced the ductility when it is used in ACCs, and this behavior will be analyzed in detail in the following section. A summary of the

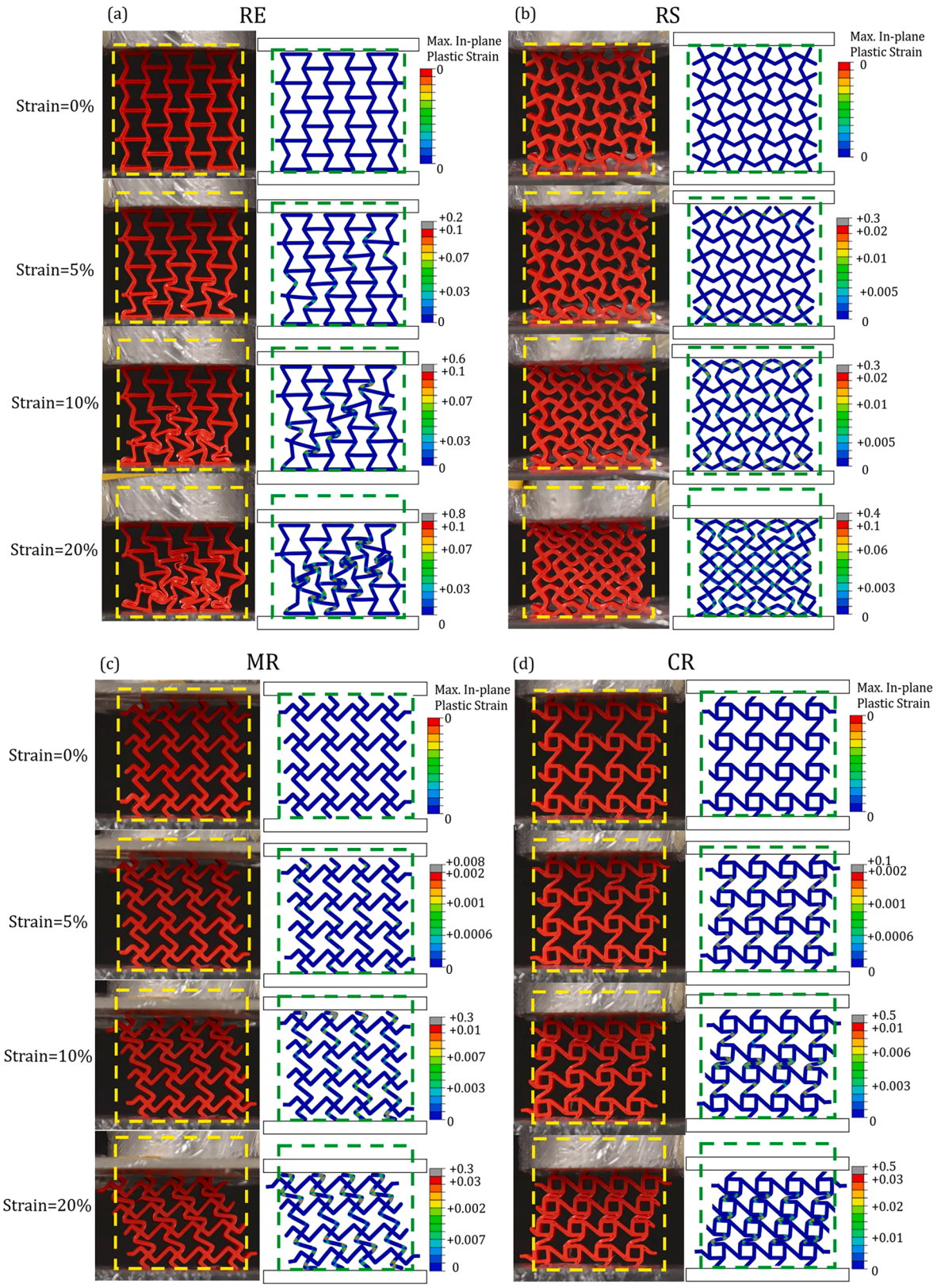

Fig. 12. Deformation and damage mode of the printed auxetic structures with increasing compressive strain a) ABS-RE, b) ABS-RS, c) ABS-CR and d) ABS-MR.

mechanical properties of the 3D printed auxetic structures is given in Table 8.

4.2. Stress–strain response of the ACCs

Conventionally, plain cementitious mortar shows brittle behavior when compressed. This was already found from the stress–strain response of the plain mortar (see Fig. 8a), as discussed in section 3.2. In

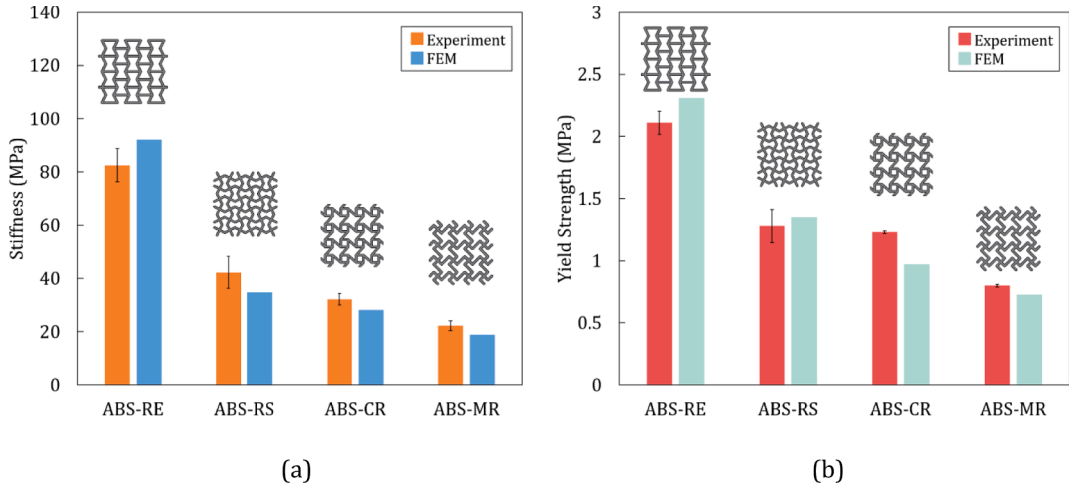

Fig. 13. Comparison of the a) stiffness, and b) yield strength of the printed auxetic structures.

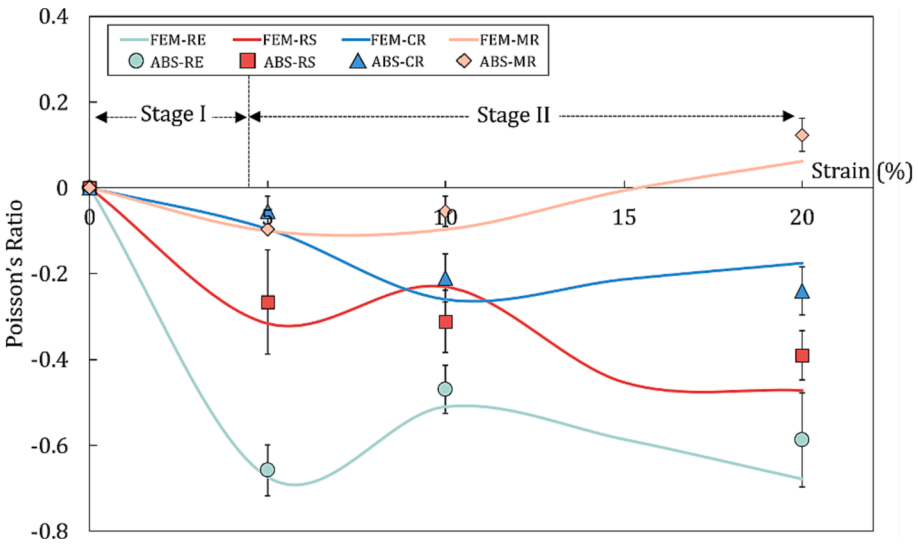

Fig. 14. Poisson's ratio of the auxetic structures obtained from experiments and numerical simulations, standard deviation is indicated.

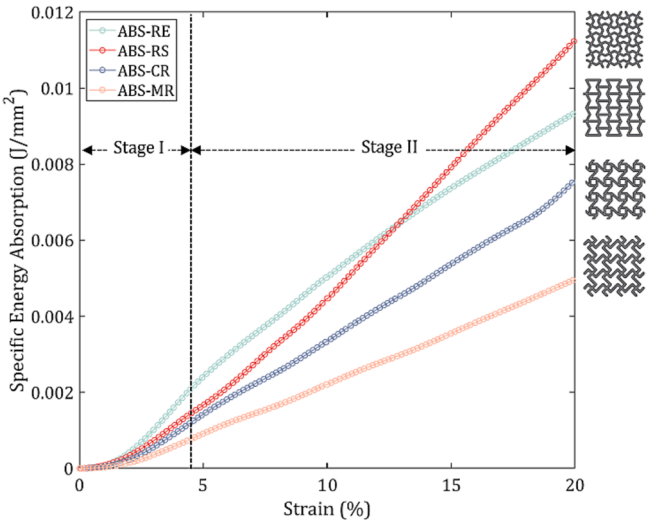

Fig. 15. Specific energy absorption of the auxetic structures.

Table 8
Mechanical properties of the ABS auxetic structures.

	Yield Strength (MPa)	Stiffness (MPa)	Specific Energy Absorption (J/mm^2)
ABS-RE	2.11	82.49	0.0094
ABS-RS	1.28	42.30	0.0113
ABS-CR	1.23	32.19	0.0075
ABS-MR	0.80	22.26	0.0050

contrast, after incorporating auxetic structures as reinforcement as done in this work, the ductility of was significantly improved. This behavior is already quite clearly indicated by the stress–strain curves of the ACCs (Fig. 16). All four types of ACCs exhibit an extremely long softening branch after the peak load (i.e., the compressive strength). This means that the ACCs was gradually damaged during the experiments, contrary to the sudden failure of the reference plain mortar.

This improvement is attributed to the auxetic behavior of the 3D printed ABS structures. Unlike the plain mortar, the auxetic behavior (lateral contraction when compressed) provides confinement to arrest the propagation of cracks. In this sense, it was difficult for the cracks to form a main cracking plane after the peak stress. Instead, multiple cracking appeared. Consequently, a long softening branch was observed

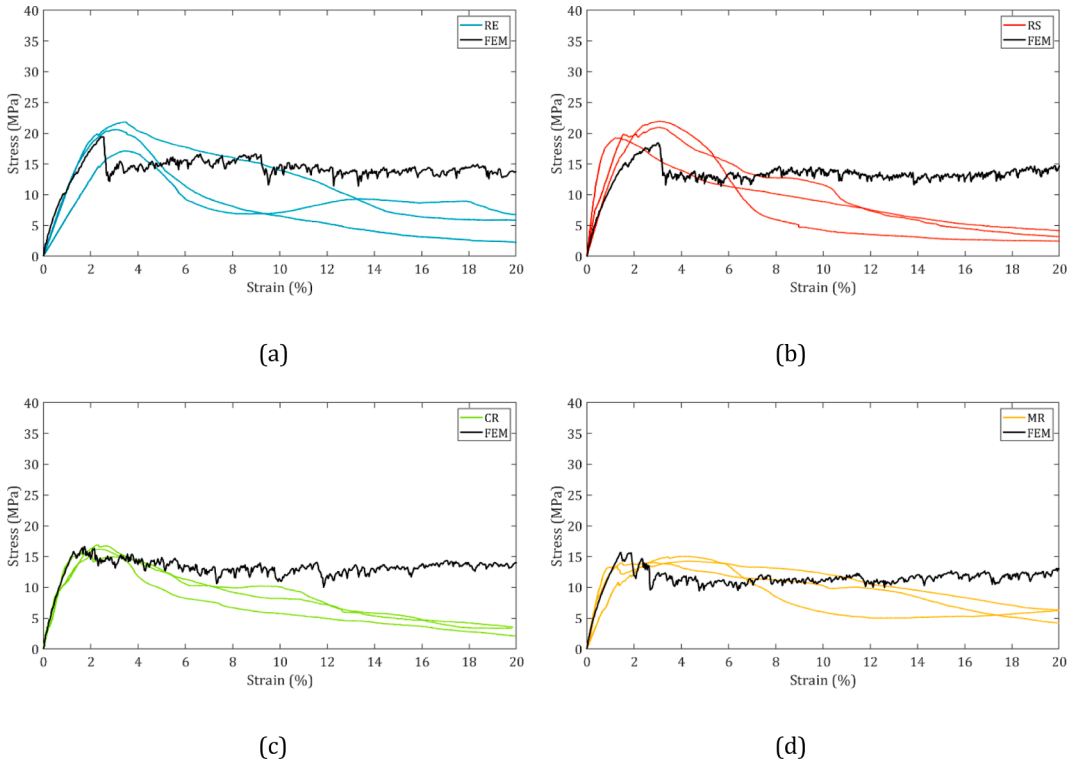

Fig. 16. Stress–strain curves of the ACCs, a)RE, b)RS, c)CR and d)MR.

in the ACCs, which therefore show much higher ductility. As seen from the DIC and simulation results in Fig. 17, the high strain regions indicate cracked locations of the ACCs. Compared to the single main cracking plane, multiple cracking regions can be seen from the damaged ACCs. This multiple cracking mechanism considerably contributes to improved ductility of the ACCs, similar to the widely known strain hardening cementitious composites.

The improved ductility can be quantitatively evaluated by the specific energy absorption. As seen in Fig. 18, the specific energy absorption of the ACCs is significantly improved compared to the plain mortar, as well as compared to the corresponding ABS auxetic structure itself. According to the experimental results, the ACCs RE, RS, CR and MR has 853 %, 817 %, 702 % and 783 % higher energy absorption than the plain mortar (REF), respectively. In the meanwhile, the ACCs also achieved 708 %, 665 %, 822 % and 1468 % higher energy absorption than the corresponding 3D printed polymeric auxetic structures. The extremely improved energy absorption proved that the proposed strategy of creating ACCs can simultaneously overcome the drawbacks of polymeric auxetic structures and cementitious mortar.

It is worth noticing from Fig. 18 that the simulated specific energy absorption obtained by the ACCs is obviously larger than the experimental values. This effect can be also found in the stress–strain curves in Fig. 16: the stress of all FEM curves stress maintained at relatively higher level than the experiment. At low strain level, the experiment and numerical model exhibit similar specific energy absorption. This can be clearly seen from Fig. 19, the absolute energy difference remains at approximately 10 %. However, as strain continues to increase the energy difference gradually increases. The specific energy absorption obtained from the numerical models is 36 %, 35 %, 50 % and 14 % higher than the experiment for RE, RS, CR and MR, respectively.

A possible reason for this mismatch could be the limitation of the 2D FEM elements. In the experiment, out-of-plain failure on the ABS auxetic structures was also observed (see, Fig. 20a) in the ACCs. This led to considerable stress decrease at higher strain level in the experiment, as witnessed by the stress–strain curves in Fig. 16. However, in the numerical models, the out-of-plain failure was not considered due the used 2D elements, therefore, the stress decrease at higher strain level was not captured by the simulation. This is a drawback of adopting 2D element in modeling mechanical properties of 3D printed materials. Using 3D models may reduce the difference, however, at a significantly higher computational cost. In contrast, the out-of-plain damage was not observed when solely compressing the 3D printed auxetic structures (see Fig. 20b); as a result, the simulated energy agrees with the experiment very well (see Fig. 18). The origin of such failure is attributed to the nature of FDM 3D printing process: weak interlayer bonding strength as clarified by a previous study [30].

On the other hand, the simulated compressive strength values show excellent agreement with the experimental results, as seen in Fig. 21. In addition, among the four tested structures the strengths of RE and RS composites are comparable to the reference plain mortar, while the CR and MR shows slightly decreased compressive strength, although they have exactly the same volumetric ratio (defined in section 2.1) as RE and RS. The difference between the four structures is attributed to their different ability to provide confinement to the ACCs. As can be seen in Fig. 22, in the pre-peak regime (at 1 % strain), the RE and RS obviously provide stronger confinement to the ACCs: inside the cells the stress is much lower. Similar confining effect was also found by [12]. In contrast, the confinement introduced by the CR and MR is not that obvious. This phenomenon emphasizes the critical impact of the auxetic pattern on the mechanical performance of the corresponding ACCs, even though they all show negative Poisson's ratio.

4.3. *Impact of volumetric ratio*

We have previously observed that the volumetric ratio (defined in section 2.1) of 3D printed reinforcement structures has huge impact on the mechanical performance of cementitious composites [7]. Similarly, this effect is also investigated in this study. We used the "rotating square" composites (RS) as an example, as the corresponding composite showed the highest compressive strength. As seen from Fig. 23, when the volumetric ratio is decreased to 14 %, the compressive strength of RS14 (black curve in Fig. 23) is obviously lower than RS (region surrounded

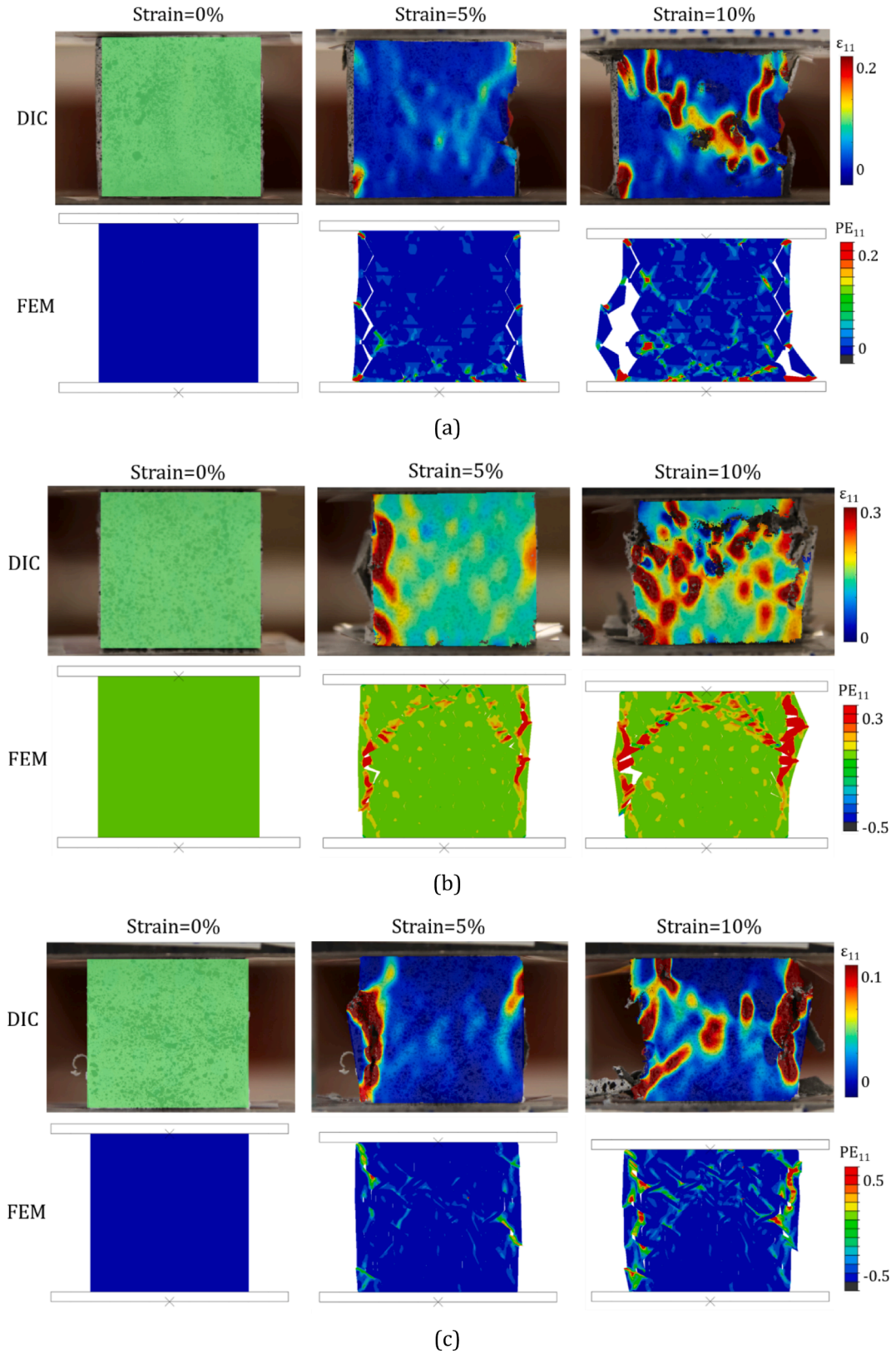

Fig. 17. Damage mode of the ACCs obtained from DIC and simulation, a) RE, b) RS, c) CR and d) MR, note that to provide bettern comparision to the DIC results, the FEM legend is not formulated based on the maximum and minimum plastic strain.

by red curves), which has 28 % of volumetric ratio.

In addition, the RS14 shows more brittle post-peak response than the RS, as indicated by a steep stress drop immediately after the peak stress on the RS14 curve (see Fig. 23). This is obviously distinct from the gradual stress decrease of the RS specimens. The main reason is the poor bond between 3D printed polymeric material and cementitious mortar.

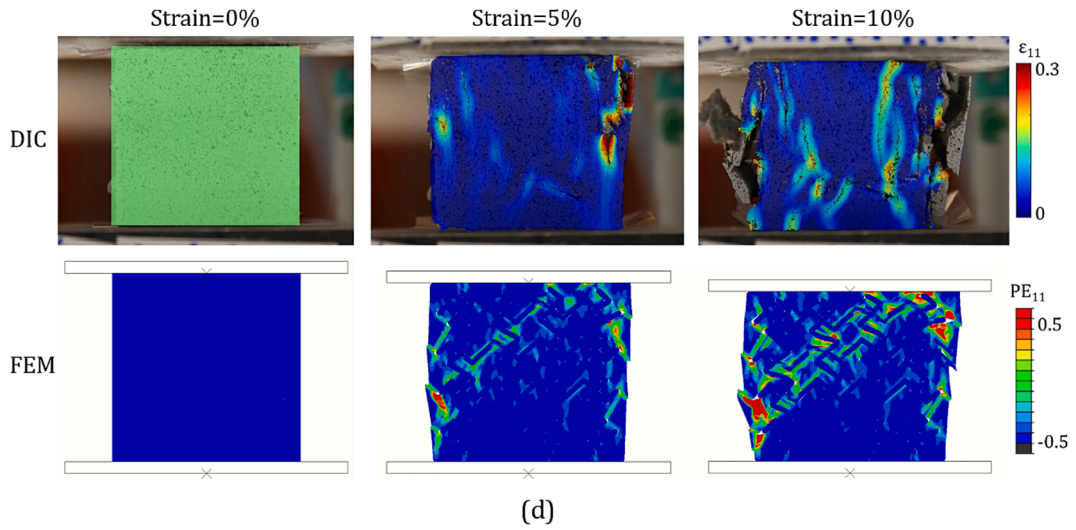

Fig. 17. (*continued*).

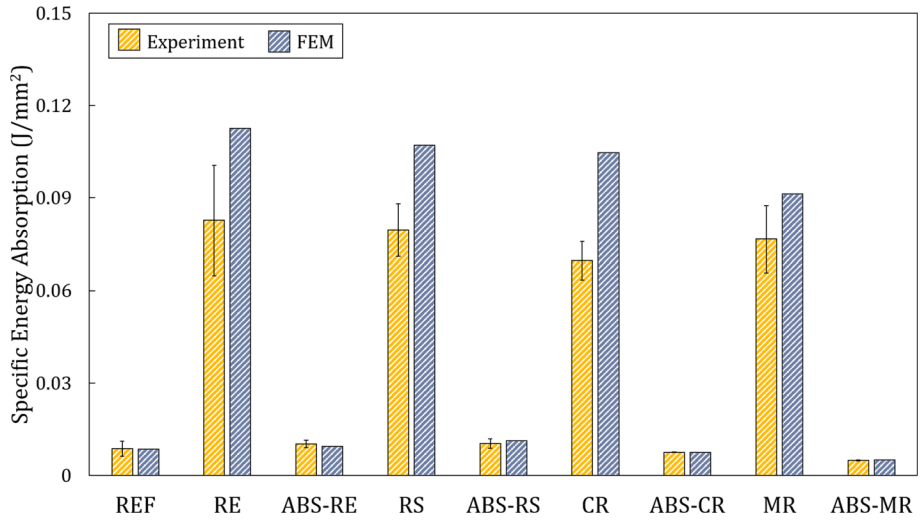

Fig. 18. Comparison of the specific enegy absorption between plain mortar, the ACCs and their corresponding ABS structures, standard deviation is indicated.

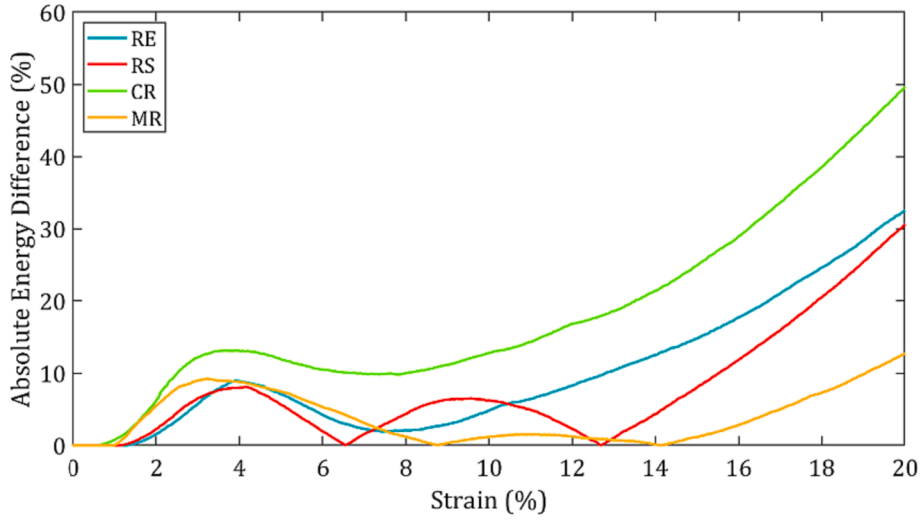

Fig. 19. Absolute value of the difference between experimentally and numerically obtained specific energy absorption.

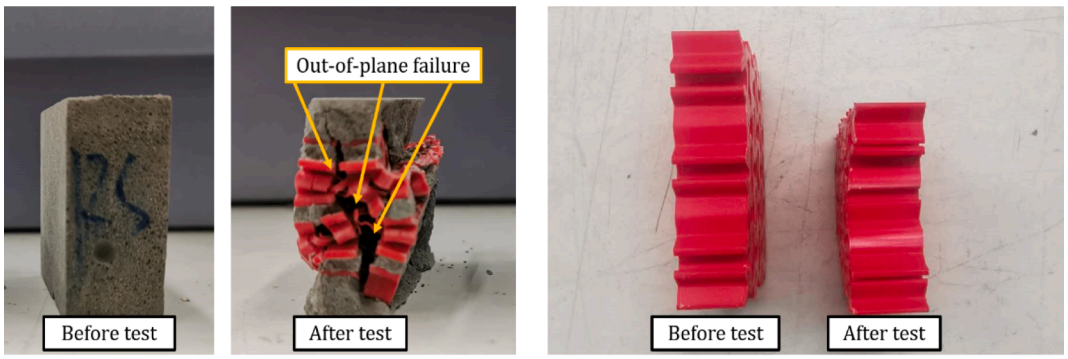

Fig. 20. Specimens before and after uniaxial compression tests; a) cementitious auxetic composite, and b) 3D printed ABS auxetic structure.

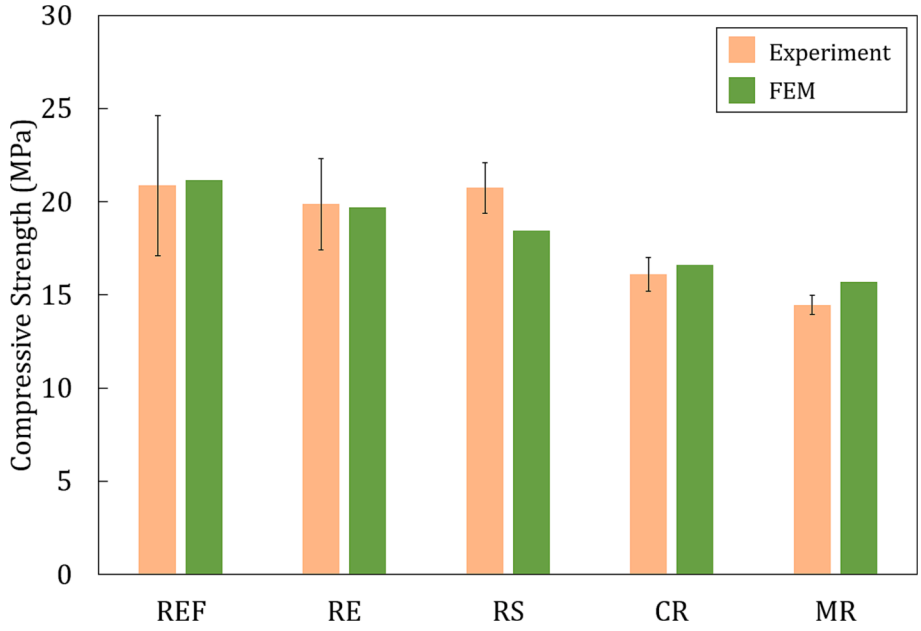

Fig. 21. Comparison of the compressive strength obtained from experiments and numerical simulations, standard deviation is indicated.

When the volumetric ratio is decreased to 14 %, two large planar contact interfaces (one side is shown in Fig. 24 by the green area) between the auxetic structure and cementitious mortar were formed on the front and back contact planes. Under compression, as soon as the stress reached the compressive strength, cracks could rapidly propagate through this contact plane, which resulted in the steep stress drop. In this sense, the bond could potentially be improved in the future thereby possibly improving the response of the composite.

Furthermore, the water-to-binder ratio of the cementitious mortar is also found to have an impact on the mechanical performance of the composites. As shown in Fig. 23, decreasing the water-to-binder ratio to 0.3 (RS14-WB3) improves the compressive strength of the composites, and the RS14-WB3 even reaches similar compressive strength as the RS. However, the steep stress drop can be still observed. As a result, the ductility of the RS14-WB3 is still obviously lower than the RS. In comparison, increasing the water-to-binder ratio to 0.5 (RS14-WB5) slightly mitigated the sharp stress drop; nevertheless, the compressive strength is significantly reduced compared to the RS.

The results obtained in the previous sections have clearly demonstrated that, even traditional steel reinforcement was not used, the 3D printed polymeric auxetic structures can significantly improve the ductility of plain cementitious mortar. The high ductility of the ACCs under compression ensures great energy absorption ability, which gives the potential of the ACCs for passive energy dissipation applications, for instance yielding support elements for squeezing tunnels which demands high compressive deformability and ductility. Furthermore, due to the planar two-dimensional geometry, the ACCs in this work may not exhibit similar high ductility under out-of-plane loadings. Under such loadings, the orientation and spatial configuration of the reinforcement auxetic structures can be altered accordingly. For instance, creating a centrosymmetric configuration using these two-dimensional auxetic structures studied in this work or even using three-dimensional auxetic structures. In these cases, though the specific damage behaviors might change due to the new configuration, and therefore needs future investigation. But the basic crack confining mechanism on the cementitious matrix induced by the auxetic structure remains similar to the findings of this study.

5. Conclusions

This work focuses on developing auxetic cementitious composites (ACCs) with enhanced mechanical properties under compression. The approach is creating a composite material which simultaneously uses cementitious material to enhance the compressive strength of polymeric

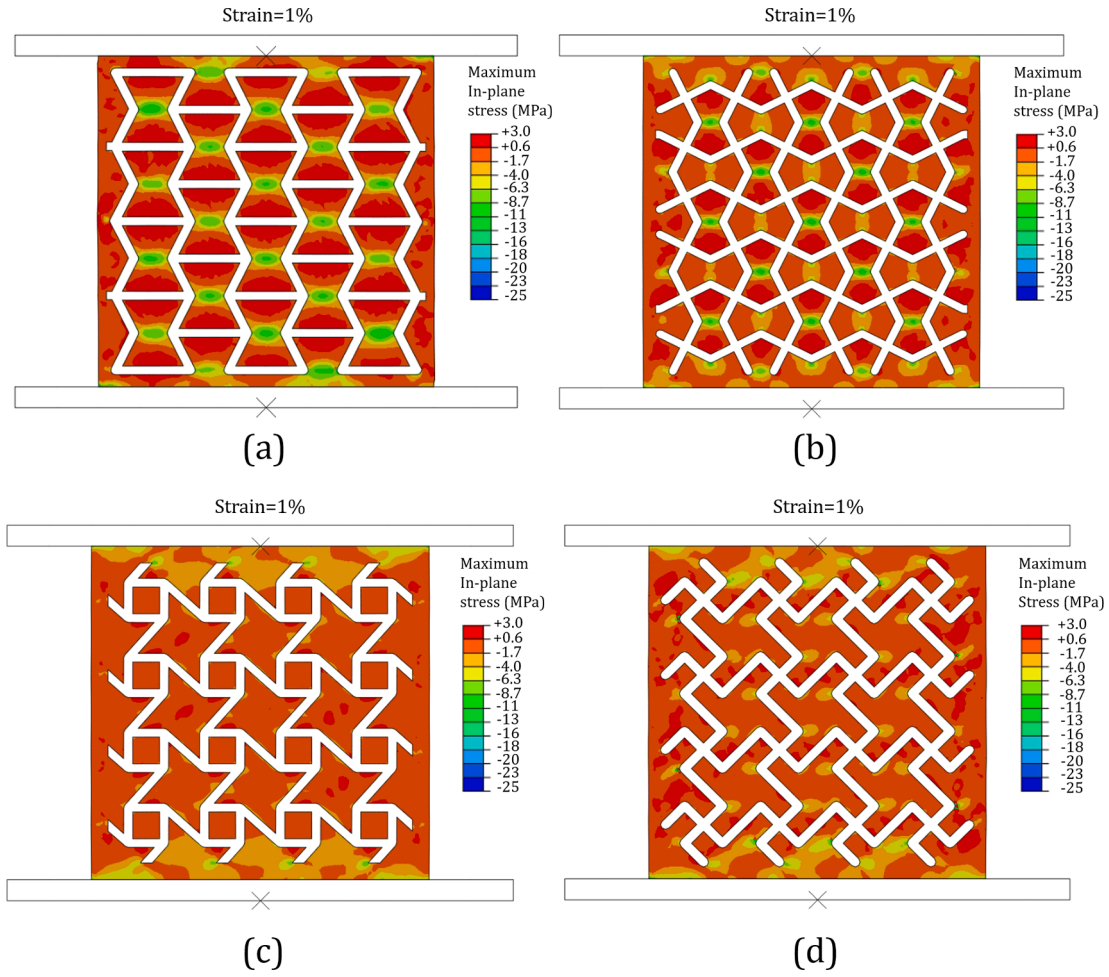

Fig. 22. Stress distribution on the ACCs in the pre-peak regime at 1% strain, a) RE, b)RS, c)CR, d)MR.

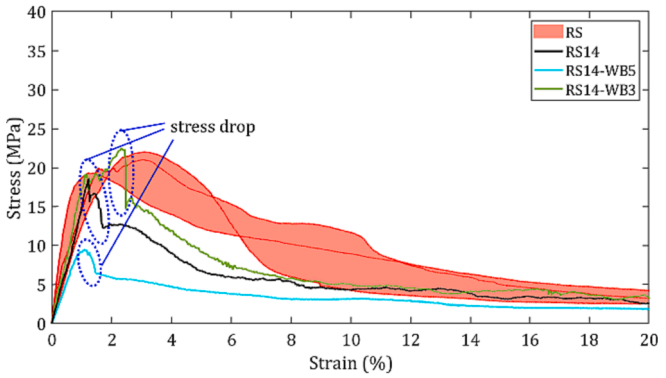

Fig. 23. Comparison of ths stress–strain curves of "rotating square" composites with different reinforcing ratio and water-to-binder ratio; note that three duplicate specimens were tested for all groups and similar behaviors were found; Only one of each curve is shown here for better contrast.

auxetic structures, and auxetic behavior to limit crack propagation in the cementitious mortar. As a further step of existing studies in this field, this work clarified the toughening mechanism of the auxetic structures in the cementitious composites through experimental and numerical tests. In addition, this work also elaborated the characteristic role of four different basic fundamental auxetic mechanisms in enhancing the ductility the cementitious materials. This could contribute to the choice and design of such auxetic reinforcement from numerous discovered

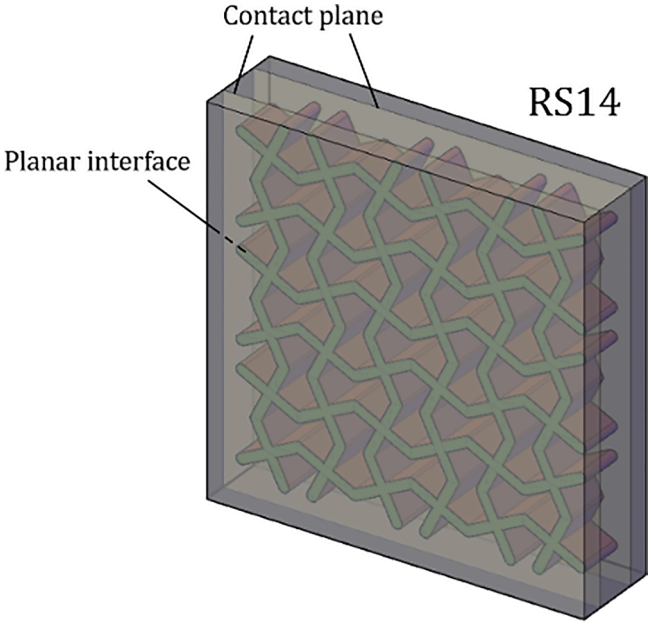

Fig. 24. Planar contact interface formed in RS14 specimen.

auxetic structures in existing literatures to create ACCs for specific engineering applications. According to the present results, several conclusions can be drawn:

- A crack-arresting toughening mechanism is found in the ACCs. The DIC and numerical simulation results suggest that the auxetic behavior of 3D printed polymeric structures provides confinement to the mortar, which arrests the post-peak crack propagation in the ACCs under compression. Therefore, all four types of cementitious auxetic composites exhibit strikingly improved ductility, quantified by the specific energy absorption. Among them, the RE shows the highest ductility which is 708 % higher than the corresponding auxetic structure and 853 % higher than the plain cementitious mortar.
- The ACCs show significantly improved compressive strength compared to the 3D printed auxetic polymeric structures. More importantly, owing to stronger confinement introduced by the auxetic behavior, the compressive strength of RS and RE is comparable to the plain cementitious mortar. In contrast, the CR and MR shows lower compressive strength than the plain cementitious mortar due to their limited crack-confining effect.
- The volumetric ratio of the auxetic structure in the composites has a critical impact on the compressive strength and ductility of the ACCs. Reducing the volumetric ratio from 28 % to 14 %, the ductility of RS decreased by 32.2 %; decreasing the water-to-binder ratio of the cementitious mortar from 0.4 to 0.3 helped to improve the compressive strength of the ACCs by 18.5 %.
- 2D finite element models can properly capture the compressive behavior of the 3D printed auxetic structures. However, they overestimate the energy absorption of the ACCs at high strain level compared to experiments. This is caused inability of 2D models to capture the out-of-plane compressive damage of the 3D printed structures in the ACCs.

Declaration of competing interest

The authors declare that they have no known competing financial interests or personal relationships that could have appeared to influence the work reported in this paper.

Data availability

Data will be made available on request.

Acknowledgements

Yading Xu and Branko Šavija acknowledge the financial support from the European Research Council (ERC) within the framework of the ERC Starting Grant Project “Auxetic Cementitious Composites by 3D printing (ACC-3D)”, Grant Agreement Number 101041342. Views and opinions expressed are however those of the author(s) only and do not necessarily reflect those of the European Union or the European Research Council. Neither the European Union nor the granting authority can be held responsible for them.

References

[1] J.G. Van Mier, Concrete fracture: a multiscale approach, CRC Press, 2012.
[2] J.G. Van Mier, Fracture processes of concrete, CRC Press, 1997.
[3] J. Gonzalez, et al., Comparison of rates of general corrosion and maximum pitting penetration on concrete embedded steel reinforcement, Cem. Concr. Res. 25 (2) (1995) 257–264.
[4] J. Sliseris, Numerical analysis of reinforced concrete structures with oriented steel fibers and re-bars, Eng. Fract. Mech. 194 (2018) 337–349.
[5] Li, V.C., From micromechanics to structural engineering-the design of cementitous composites for civil engineering applications. 1993.
[6] H.R. Pakravan, M. Latifi, M. Jamshidi, Hybrid short fiber reinforcement system in concrete: a review, Constr. Build. Mater. 142 (2017) 280–294.
[7] Y. Xu, B. Šavija, Development of strain hardening cementitious composite (SHCC) reinforced with 3D printed polymeric reinforcement: mechanical properties, Compos. B Eng. 174 (2019), 107011.
[8] Y. Xu, et al., Cementitious composites reinforced with 3D printed functionally graded polymeric lattice structures: experiments and modelling, Addit. Manuf. (2021), 101887.
[9] B. Salazar, et al., Polymer lattice-reinforcement for enhancing ductility of concrete, Mater. Des. 196 (2020), 109184.
[10] V. Nguyen-Van, et al., Performance of concrete beam reinforced with 3D printed Bioinspired primitive scaffold subjected to three-point bending, Autom. Constr. 134 (2022), 104060.
[11] A. Skoratko, et al., Mechanical properties of mortar beams reinforced by gyroid 3D printed plastic spatial elements, Cem. Concr. Compos. 134 (2022), 104809.
[12] V. Nguyen-Van, et al., Dynamic responses of bioinspired plastic-reinforced cementitious beams, Cem. Concr. Compos. 133 (2022), 104682.
[13] C. Tang, et al., Flexural properties of 3D printed graded lattice reinforced cementitious composites using digital image correlation, Mater. Des. 227 (2023), 111734.
[14] Xu, Y., B. Šavija, and E. Schlangen. Compression Behaviors Of Cementitious Cellular Composites With Negative Poisson’s Ratio. in FramCos. 2019. France.
[15] C. Zhao, et al., Experimental study and finite element analysis on energy absorption of carbon fiber reinforced composite auxetic structures filled with aluminum foam, Compos. Struct. 303 (2023).
[16] X. Zhang, et al., Quasi-static compression and dynamic crushing behaviors of novel hybrid re-entrant auxetic metamaterials with enhanced energy-absorption, Compos. Struct. 288 (2022).
[17] X. Cheng, et al., Design and mechanical characteristics of auxetic metamaterial with tunable stiffness, Int. J. Mech. Sci. 223 (2022).
[18] R. Johnston, Z. Kazancı, Analysis of additively manufactured (3D printed) dual-material auxetic structures under compression, Addit. Manuf. (2021) 38.
[19] X.G. Zhang, et al., A novel auxetic chiral lattice composite: Experimental and numerical study, Compos. Struct. 282 (2022), 115043.
[20] A. Airoldi, et al., Foam-filled energy absorbers with auxetic behaviour for localized impacts, Mater. Sci. Eng. A 788 (2020).
[21] W. Wu, et al., Mechanical design and multifunctional applications of chiral mechanical metamaterials: a review, Mater. Des. 180 (2019), 107950.
[22] J.N. Grima, K.E. Evans, Auxetic behavior from rotating squares, J. Mater. Sci. Lett. (2000).
[23] J.N. Grima, K.E. Evans, Auxetic behavior from rotating triangles, J. Mater. Sci. 41 (10) (2006) 3193–3196.
[24] J.N. Grima, et al., Auxetic behaviour from rotating semi-rigid units, Physica Status Solidi (b) 244 (3) (2007) 866–882.
[25] M. Chen, et al., Static and dynamic compressive behaviour of 3D printed auxetic lattice reinforced ultra-high performance concrete, Cem. Concr. Compos. 139 (2023), 105046.
[26] R. Zhong, et al., Mechanical properties of concrete composites with auxetic single and layered honeycomb structures, Constr. Build. Mater. 322 (2022), 126453.
[27] J.A. Rosewitz, H.A. Choshali, N. Rahbar, Bioinspired design of architected cement-polymer composites, Cem. Concr. Compos. 96 (2019) 252–265.
[28] C.W. Smith, J.N. Grima, K. Evans, A novel mechanism for generating auxetic behaviour in reticulated foams: missing rib foam model, Acta Mater. 48 (2000).
[29] J.N. Grima, R. Gatt, P.-S. Farrugia, On the properties of auxetic meta-tetrachiral structures, Physica Status Solidi (b) 245 (3) (2008) 511–520.
[30] Y. Xu, et al., Deformation and fracture of 3D printed disordered lattice materials: experiments and modeling, Mater. Des. 162 (2019) 143–153.
[31] J.M. Chacón, et al., Additive manufacturing of PLA structures using fused deposition modelling: effect of process parameters on mechanical properties and their optimal selection, Mater. Des. 124 (2017) 143–157.
[32] A.R. Torrado, et al., Characterizing the effect of additives to ABS on the mechanical property anisotropy of specimens fabricated by material extrusion 3D printing, Addit. Manuf. 6 (2015) 16–29.
[33] Y. Xu, et al., Tunable mechanical behavior of auxetic cementitious cellular composites (CCCs): experiments and simulations, Constr. Build. Mater. 266 (2021), 121388.
[34] Dassault, Abaqus documentation. 2017. **Concrete damaged plasticity**(https://abaqus-docs.mit.edu/2017/English/SIMACAEMATRefMap/simamat-c-concretedamaged.htm).
[35] Z. Wu, Y. Xu, B. Savija, Mechanical properties of lightweight cementitious cellular composites incorporating micro-encapsulated phase change material, Materials (basel) 14 (24) (2021).
[36] Systemes, D., Abaqus.pdf. 2008.
[37] V. Nguyen-Van, et al., Bioinspired cellular cementitious structures for prefabricated construction: hybrid design & performance evaluations, Autom. Constr. 119 (2020), 103324.
[38] Y. Xu, et al., Cementitious cellular composites with auxetic behavior, Cem. Concr. Compos. 111 (2020), 103624.
[39] N. Chikkanna, et al., Quasi-static compression performance of material extrusion enabled re-entrant diamond auxetic metamaterial: Fabrication, tuning the geometrical parameters and fibre reinforcements, Thin-Walled Struct. 179 (2022).